J Electroceram (2010) 24:245–260
DOI 10.1007/s10832-009-9565-z

Analyzing results of impedance spectroscopy using novel evolutionary programming techniques

A. B. Tesler · D. R. Lewin · S. Baltianski · Y. Tsur

Received: 30 January 2008 / Accepted: 16 January 2009 / Published online: 12 February 2009

Abstract This paper discusses the application of evolutionary programming methods to the problem of analyzing impedance spectroscopy results. The basic approach is a "direct-problem" one, i.e., to find a time constant distribution function that would create similar impedance results as the measured ones, within experimental error. Two complementary methods have been applied and are discussed here: Genetic Algorithm (GA) and Genetic Programming (GP). A GA can be applied when a known (or desired) model exists, whereas GP can be used to create new models where the only a-priori knowledge is their smoothness and their non-negativity. GP is tuned to prefer relatively non-complex models through penalization of unnecessary complexity.

Keywords Impedance spectroscopy · Evolutionary programming · Genetic algorithm · Genetic programming

1 Introduction

1.1 Impedance spectroscopy

In recent years, there has been increasing interest in the investigation of complex systems exhibiting a wide range of relaxation time behavior [1]. Such systems can be found in various areas of science and engineering, for example in solid-state electrochemistry [2, 3], device manufacturing [4], fuel cells [5], applied electrochemistry [1, 6, 7] and corrosion phenomena [8–10]. While Impedance Spectroscopy (IS) is a very sensitive technique, the data provided by the experiment are hard to deal with. The main reason is that it is an inverse problem in which: (a) the measured signal contains noise; (b) the range of available frequencies is finite; and (c) the number of data points is finite and the measurements are discrete rather than continuous. Since there are an infinite number of models that can fit the data, the identification of "the best" model is therefore an ill-posed inverse problem, which mathematically can be expressed by a Fredholm integral equation [11]. Several methods have been proposed to solve the IS problem [12]. Among them are the Marquardt–Levenberg search algorithm [2], modified Tikhonov regularization [13], the Monte-Carlo method [14], Fourier transformation along with extrapolation and filtering [15], and fitting an equivalent circuit to experimental results [16–18]. Some of the equivalent circuit searches do that by applying genetic algorithms [19–21].

The most widely used method to analyze ac impedance data is by constructing an equivalent circuit containing lumped and/or distributed elements that generate a similar impedance spectrum to that of the measured experimental data. It is sometimes possible to relate these values and changes in them to specific parts of the system and interpret the processes that occur within. In addition, it is also possible to consider deconvoluting the data in an attempt to explain the experimental results by examining each region separately [22, 23].

The degree of inhomogeneity exhibited by a sample under test (SUT) can be enormous. In principle, since IS is an integral measurement in nature, its validity is enhanced insomuch as the sample is homogeneous. Additional difficulty arises from the possibility of frequency-dependant current lines in the sample, especially at low frequencies

A. B. Tesler · D. R. Lewin · S. Baltianski · Y. Tsur (✉)
Department of Chemical Engineering, Technion, IIT,
Haifa 32000, Israel
e-mail: tsur@tx.technion.ac.il

[24]. Evidently, an equivalent circuit with a finite number of electrical elements cannot be expected to describe all the occurring phenomena in a SUT. In addition, it is well-known that many different configurations of equivalent circuits can provide exactly the same impedance data over the whole range. Hence one of the dangers in equivalent circuits is that we would be tempted to believe the over-information they provide. Hence we prefer to search for the best distribution of relaxation times (DRT), but the following methods can be implemented for equivalent circuits as well.

This article suggests a novel approach to solve the impedance spectroscopy inverse problem based on evolutionary programming methods. The two methods that are discussed here are GA and GP (see below). GA can be regarded as yet another fitting method. However, it is a very useful method when the fitting task is to find a function that its convolution would fit the experimental data, as compared to fitting directly a known function to the data. GP is a new concept in IS that does not fit a known function (i.e., finds parameters) but rather finds new functions. This is done on the expense of much longer computer resources, and we recommend using it for new materials and problems. GP is particularly useful in IS to eliminate the limitations based on the preliminary choice of one or very few models. It reduces the influence of the subjective approach of the researcher, and keeps the chance of finding new, perhaps odd or less predictable mathematical models. These features are most important in the research of completely new objects and also for known objects under the influence of extraordinary conditions.

1.2 Evolutionary programming

From the beginning of the 1980's, evolutionary-based optimization algorithms, using mechanisms inspired by biological evolution, were introduced [25, 26], and implemented in large number of applications [27–29]. Today, two main evolutionary programming methods are widely used: Genetic Algorithms (GA) and Genetic Programming (GP). While Genetic Algorithms deal with a fixed structure of a proposed model, evolving optimal values of its numerical parameters, Genetic Programming is a more general evolutionary computing approach with no fixed structure, allowing the evolutions of both the structure and the numerical parameters of a model. Both approaches are typically implemented as computer programs in which a population of abstract representations (chromosomes) of candidate solutions (individuals) to an optimization problem evolves toward better solutions. The evolution is usually initiated from a population of completely random individuals, which evolve over generations. In each generation, the fitness of each individual in the population is evaluated, multiple individuals are selected from the current population (based on their fitness), and are modified by evolutionary operators (for example, mutation and crossover) to form a new population. The new population is then used in the next iteration of the algorithm. The main difference between GP and GA is the search space of the solution; in contrast to the fixed model structure used in a GA, GP evolves the structure of the model using simple mathematical functions such as sine, cosine, exponent and terminals as summation, subtraction, multiplication and division, as well as its numerical parameters. Despite the fact that GP is computationally intensive, the exponential growth of CPU power in the last decades and various improvements in GP technology enable its implementation in many fields of science and engineering [27–31].

Here we present software developed to quantify the noise of measured IS data and to find the most compact models that fit the data well enough using GA and GP. The first method facilitates robust parameter estimation for a given model, while the second uses an adaptive GP approach [32, 33] to create relatively non-complex models. The latter is done by penalization for both the complexity of the model and discrepancies between the experimental data and the predictions of the model.

2 Experimental

Figure 1 schematically represents the devices in the IS experiment, used in our laboratory. A sample is located either in the furnace or in the cryostat, to allow temperature

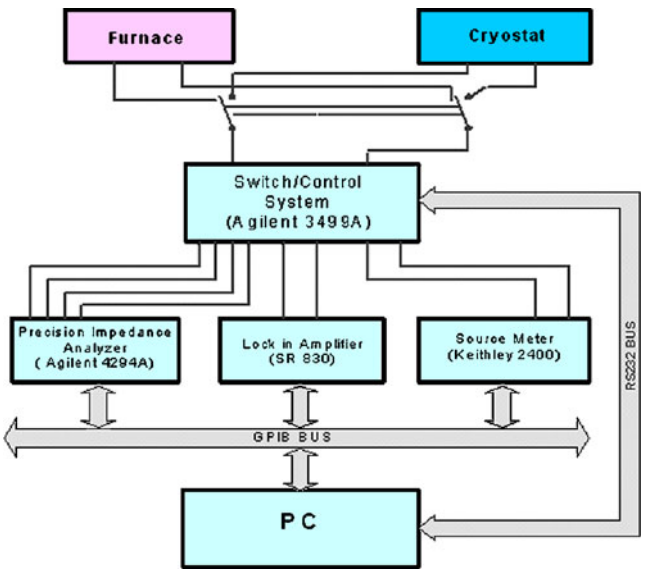

Fig. 1 Schematic representation of the IS experiment

control. In our laboratory, IS experiments were carried out by employing two measurement instruments [34]: Lock-in Amplifier for lower frequencies (SR 830, Stanford Research Systems) and Precision Impedance Analyzer for higher frequencies (Agilent 4294A).

3 Programming

3.1 Data validation using Kramers–Kronig transforms

The Kramers–Kronig relations (K–K) [35, 36], that are a special form of Hilbert relations [37, 38], couple the real and imaginary parts of the complex dielectric function. This is a result of the causal nature of the response of materials to external stimulus. For the experimental results to be valid, four conditions must be fulfilled: (a) causality, (b) linearity, (c) stability and (d) finite-valueness [39–41].

The K–K relations that transform the imaginary part of an electrochemical system to the real part and vice versa are written as:

$$Z''_{\mathrm{KKT}}(\omega) = -\left(\frac{2\omega}{\pi}\right)\int_0^\infty \frac{Z'_{\mathrm{meas}}(x) - Z'_{\mathrm{meas}}(\omega)}{x^2-\omega^2}dx \qquad (1)$$

$$Z'_{\mathrm{KKT}}(\omega) - Z'_{\mathrm{meas}}(\infty) = \left(\frac{2}{\pi}\right)\int_0^\infty \frac{x\cdot Z''_{\mathrm{meas}}(x) - \omega\cdot Z''_{\mathrm{meas}}(\omega)}{x^2-\omega^2}dx \qquad (2)$$

Here, x denotes the frequency point as the integrand. Equation 2 can be simplified, at least for dielectric materials between metal electrodes, in the common cases where $Z'_{\mathrm{meas}}(\infty)$ equals zero. The polarization resistance of the sample can be directly estimated from the resistive part if the measured bandwidth is large enough and asymptotic behavior at low frequencies can be clearly observed. If the asymptotic behavior of the resistive component does not observed, the polarization resistance can be calculated indirectly from the reactive component by employing Eq. 2 (again, for cases where $Z'_{\mathrm{meas}}(\infty)$ equals zero), at angular frequency ω equals zero.

The typical IS experiment provides discrete experimental data recorded at logarithmically-spaced frequency intervals, consisting of resistive and reactive components. Consequently, integration of Eqs. 1 and 2 can neither be carried out analytically nor over the infinite frequency bandwidth. The values of the apparent singular point at each calculation step in Eqs. 1 and 2 can be calculated by employing l'Hopital's rule [42]. Average Error [40, 43] (AE) is calculated and determines the validity of the measured impedance data (see Appendix).

3.2 Stating the problem

The dielectric polarization in many materials cannot be described by a single relaxation time (τ_D) but rather by a distribution of relaxation times (DRT) $G(\tau)$:

$$Z(\omega) = R_{\mathrm{pol}}\int_0^\infty G(\tau)K(\omega,\tau)d\tau, \qquad (3)$$

where τ represents the relaxation time and $G(\tau)d\tau$ is the fraction of relaxation processes between times τ and $\tau + d\tau$. As explained above, R_{pol} can either be calculated using the K–K relation or by an asymptotic extension of the resistive impedance component. In addition, $G(\tau)$ has to satisfy the normalization condition:

$$\int_0^\infty G(\tau)d\tau = 1. \qquad (4)$$

$K(\omega, \tau)$ is a kernel function that in principle is known from theory, taken here as the Debye kernel:

$$K(\omega,\tau) = \frac{1}{1+j\omega\tau}\cdot \qquad (5)$$

It is convenient to represent the DRT function in logarithmic space, with appropriate changes in the integration limits:

$$Z(\omega) = R_{\mathrm{pol}}\int_{-\infty}^\infty \frac{\Gamma(\log\tau)}{1+j\omega\tau}d(\log\tau)\cdot \qquad (6)$$

where the distribution satisfies the condition: $\int_0^\infty G(\tau)d\tau = \int_{-\infty}^\infty \Gamma(\log\tau)d(\log\tau) = 1\cdot$ Our problem is to find "the best" distribution function.

3.3 Genetic algorithm

In genetic algorithm IS analysis (IS-GA), the user selects a model, while the program optimizes all of its parameters. To be valid, the DRT function must be: (a) continuous, (b) real, (c) non-negative and (d) finite at the margins. These constraints still allow a great number of models, as indicated by the large variety of those suggested previously [7, 14, 27, 44, 45]. Wagner was the first to propose models of a Gaussian distribution function of the following form [14]:

$$\Gamma(\log\tau) = \frac{\rho}{\sigma\sqrt{2\pi}}exp\left(\frac{-(log\,\tau - log\,\tau_0)^2}{2\,\sigma^2}\right) \qquad (7)$$

where τ_0 represents the central position of the time constant, σ is a standard deviation of the distribution and ρ is a weight parameter for cases where more than a single Gaussian is present. The Gaussian distribution function provides a good fit to the response of materials with dipole–

dipole interactions. Hence, Eq. 6, describing the impedance complex function, was combined with Eq. 7 as the objective function and implemented in IS-GA. However, it is impossible to calculate the impedance integral between minus and plus infinity due to the fact that measurement instruments have limited frequency bandwidth. Moreover, in many experiments the presence of more than one peak can be observed. In such cases, superposition of Gaussian models as relaxation-time distribution functions could be applied. Hence, the general form of the impedance functions in our IS-GA code was:

$$Z(\omega) = R_{\text{pol}} \int_{\min(\log\tau)}^{\max(\log\tau)} \frac{\sum_{i=1}^{n} \frac{\rho_i}{\sigma_i\sqrt{2\,\pi}} \exp\left(-\frac{(\log\tau-\log\tau_{0i})^2}{2\sigma_i^2}\right)}{1+j\omega\tau} d(\log\tau) \tag{8}$$

There are three numerical parameters in each Gaussian term in the model that have to be evaluated: magnitude, standard deviation and peak or time constant position. This definite integral can be obtained using numerical integration; Simpson's rule was implemented in the IS-GA code.

3.3.1 Fitness function as implemented in the IS-GA

A fitness function is a particular type of objective function that quantifies the optimality of a solution in a GA, enabling competing chromosomes to be ranked. Optimal chromosomes, or at least chromosomes which are more optimal, are allowed to breed and mix their datasets by one or more techniques, producing a new generation that will (hopefully) be even better. The objective function of the IS-GA is based on the prediction resulted from the DRT function, computed for each individual solution in the population. Modified Complex Non-Linear Least Squares [46] (m-CNLS) analyzes the fitness between the suggested model and the experimental data. Here we have introduced a weighting parameter, $0 \le \phi \le 2$, which can be either a constant chosen by the user or a free parameter. It defines to what extent the deviations will be considered relative to the measurements. For instance, when ϕ is 0 the summation is of the square of the deviations whereas when ϕ is 2 the summation is of the square of the relative deviations. Our recommendation here is that the user would get some experience with the specific system and then decide for a constant value that will be set for ϕ in all the analyses of that system.

$$\begin{aligned} \text{m}-\text{CNLS} = {} & \frac{b}{\left\langle\left|Z''_{\text{calc}}(\omega)\right|\right\rangle^{2-\phi}} \cdot \sum \frac{\left(Z''_{\text{calc}}(\omega)-Z''_{\text{meas}}(\omega)\right)^2}{\left(\left|Z''_{\text{calc}}(\omega)\right|\right)^{\phi}} + \\ & + \frac{1-b}{\left\langle\left|Z'_{\text{calc}}(\omega)\right|\right\rangle^{2-\phi}} \cdot \sum \frac{\left(Z'_{\text{calc}}(\omega)-Z'_{\text{meas}}(\omega)\right)^2}{\left(\left|Z'_{\text{calc}}(\omega)\right|\right)^{\phi}} \end{aligned} \tag{9}$$

Here, Z'_{calc} and Z''_{calc} are the resistive and reactive components of the impedance computed for each model, Z'_{meas} and Z''_{meas} are the resistive and reactive components of the impedance for the experimental data set, and b is a weighting factor. Ideally, for data that perfectly obey the KK transforms, one can settle for checking the fitness of either the imaginary or the real part only (b=1 or b=0 respectively). In reality, one should check the fitness of both parts, i.e., choose a value in between those limiting cases. The weighting factor, b, is defined in advance by the user and is kept constant during the calculation.

To overcome potential difficulties when initializing the population, the user determines an upper m-CNLS limit. Only randomly-generated individuals with lower m-CNLS values are included in the initial population. In the IS-GA, random number sets are created by Matlab® engine as model parameters.

Each measured point is the result of the averaging of a number of sinusoidal signal cycles at steady state. At low frequencies, the number of such cycles is particularly low and, consequently, the experimental data are noisier. In order to alleviate this problem, the m-CNLS criterion is multiplied by a filter:

$$\text{filter} = \left(1+\exp\frac{-5(\log\omega-\log\omega_0)}{\log\omega_1-\log\omega_0}\right)^{-1} \quad , \quad \omega_1 > \omega_0 \tag{10}$$

Here the following constants have to be defined by the user: $\log(\omega_0)$ corresponds to the frequency where the filter equals 0.5, and $\log(\omega_1)$ signifies the frequency where the filter is almost 0.99, and hence is a measure of the slope or width of the filter.

3.4 Genetic programming

To create new DRT functions, IS-GP uses simple mathematical functions and terminals as listed below:

Mathematical functions: Exp(x); Sqrt(x); $\text{Log}_{10}(x)$; Exp($-x^2$); Sinh(x); Sin(x); Cos(x); $1/(1\pm x)$; and Cosh(x).

Terminals: summation (+); subtraction (−); multiplication (*); division (/); square (^2); and power (^).

An initial population of models is generated randomly using the mathematical functions and terminals mentioned above, with preset probabilities of occurrences. In addition to the two genetic operations that are used in the IS-GA procedure (crossover and mutation), two additional operations are implemented to reproduce new offsprings in IS-GP. The concept of permutation expresses the idea that distinguishable objects may be arranged in various different orders. Hence, *permutation* is a genetic operation used to rearrange the parent genetic data that are contained in a

Table 1 Gaussian model parameters that were used to create synthetic data sets according to Eq. 8 with addition of about 3% noise.

ρ_i	σ_i	$\log_{10}(\tau_{0i})$	R_{pol}
0.6	0.7	−0.5	10
0.4	0.3	−2.5	

chromosome. Another evolutionary GP operation (mutation) that does not exist in GA is the *replacement* of any part of the suggested model structure by a constant. The user defines the probability of appearance of these operations before the computation begins.

In contrast to the genetic algorithm that manipulates only the numerical values of the model parameters, the GP code tackles the problem of IS by selection of the DRT model and its complexity and determination of its parameters automatically. Here, the IS-GP code evolves the DRT function, by putting together the simple mathematical functions and terminals that were listed above. R_{pol} is included in the DRT function and is fitted together with it. The DRT function has to satisfy the conditions listed previously over the entire frequency bandwidth just by combining all mathematical functions and terminals. Because the typical impedance experiment provides data over a finite frequency range; the optimization algorithms fit it only in a specific region. Hence, if GP is treated without caution, it can generate models that fit the experimental range quite nicely, but are most probably not physical. To demonstrate this, we have generated synthetic data using again Eq. 8 with parameters that are listed in Table 1. Running GP without limitations yielded a DRT function shown by the solid line in Fig. 2. Note that IS-GP fits the synthetic impedance data and not the DRT functions directly. The synthetic DRT (shown by points in Fig. 2) and the function generated by IS-GP are remarkably

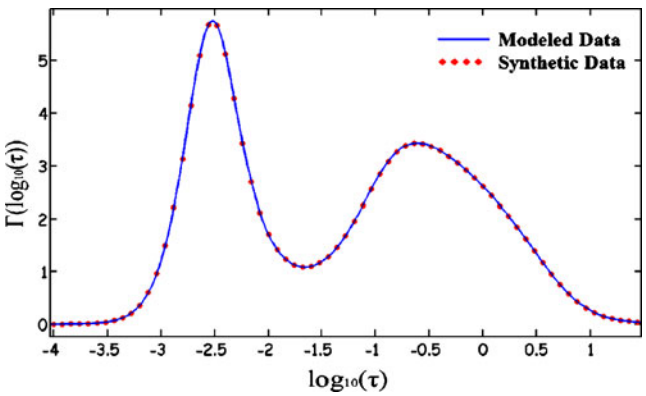

Fig. 2 DRT function fitted by genetic programming in the given finite frequency range

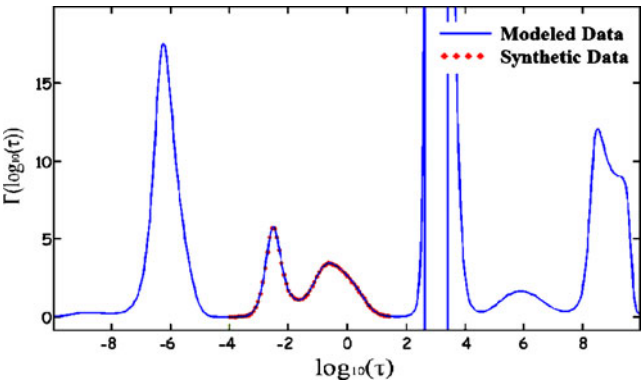

Fig. 3 The same DRT function as in Fig. 2, extrapolated to log $\tau \rightarrow \pm 10$

similar. However, it can be clearly observed from Fig. 3 that the extrapolated DRT function in this case has negative values and is discontinuous. We therefore seek to create physically-possible models of the DRT function using extrapolated frequency bandwidth, and modified the IS-GP accordingly. In the IS-GP code, the DRT function is created and the conditions are tested in the range between 10^{-20} Hz as the lower frequency limit and 10^{20} Hz as the higher frequency limit. Those limits can definitely be considered as practically "infinite", since 10^{-20} Hz has period which, according to our present knowledge, is much more than the age of the universe, while 10^{20} Hz is in the gamma rays region. This feasibility test is applied to each solution proposed by the IS-GP algorithm, and infeasible solutions are eliminated. The GP then evolves the models by applying *all* the genetic operators described previously.

Each approved model is combined with parameters and then sent to the optimizer. The idea is to add the degrees of freedom to an optional model structure [32]. An example of this concept is shown schematically by Fig. 4. The method

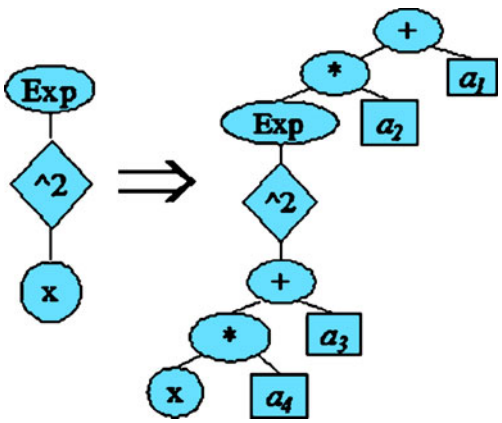

Fig. 4 Schematic representation of adding the degrees of freedom to the given model

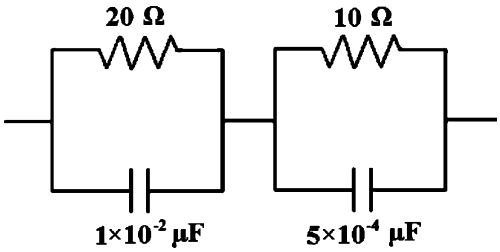

Fig. 5 Voigt equivalent circuit provides the K–K transformable impedance data

is based on the ability of the algorithm to identify the tree structure of the suggested model. The figure shows an example of a proposed model (left) and the function that is sent accordingly to the optimizer (right). Here, a_1, a_2, a_3 and a_4 can be either positive or negative constants. For each model in the solution population, the algorithm carries out a nonlinear least-squares fit to determine the values of the model parameters that minimize the prediction error. The approach described by Grosman and Lewin [33] was used. An additional feature of the IS-GP algorithm is that the objective function of the optimization process also takes into consideration the DRT's first derivative. This strategy reduces further the possibility of creating unfeasible models.

The fitness function is certainly one of the most important components in GP calculations. A fitness function quantifies the optimality of a solution (chromosome) in GP and ranks it against all the other chromosomes. To do so, this function is designed to trade-off between the complexity and the fitness of the particular model. To avoid over-fitting, the fitness of a model is determined by considering two independent experimental data sets. The first data set is used by the algorithm for fitting, i.e., to determine the model's parameters. The fitness of the model as compared to this data set is called the modeling fitness, f_M. Then a second fitness that reflects the difference between the model and the second experimental data set is calculated. This fitness parameter is called the prediction fitness, f_P. Both the modeling and the prediction fitness parameters vary from zero (for no fitness) to one (for perfect fitness). The actual fitness, f, is based on penalty for complexity of the model and a weighted sum of f_M and f_P:

$$f = \frac{\alpha \cdot f_M + (1-\alpha)\cdot f_P}{1 + e^{\lambda(n_c-(M_c-\beta))}} \tag{11}$$

In Eq. 11, α is the fraction of the fitness value calculated on the basis of the modeling fitness, and the denominator is a sigmoid shaped adaptive function that allows the penalization of over-complex models. The shape of this sigmoid is controlled by its parameters: λ being a constant that determines the slope of the complexity constraint sigmoid; n_c is the complexity of the inspected model, which is equal to the number of its branches; M_c is the best model complexity of the previous generation; and β is a constant responsible of the ability of the algorithm to accept solutions of greater complexity than M_c. More details are given in Grosman and Lewin [33].

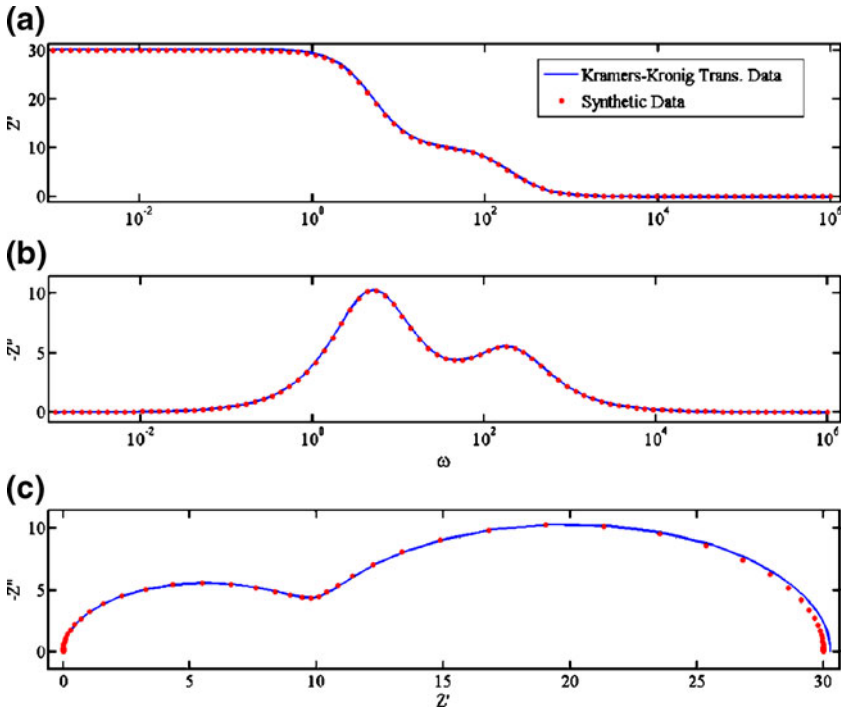

Fig. 6 K–K transformed impedance spectra created with 0.1 log (f/Hz) intervals: (**a**) the impedance imaginary part vs. logarithmic angular frequency, (**b**) the impedance real part vs. logarithmic angular frequency, (**c**) the Cole–Cole diagram

Table 2 Average errors of the K–K transforms computation.

Transformation	AE value [%] with intervals 0.1 [log(f/Hz)]	AE value [%] with intervals 0.05 [log(f/Hz)]
Real-to-imaginary	0.1869	0.0361
Imaginary-to-real	0.4202	0.0675
Polarization resistance	0.8929	0.1689

When two different models fit the data similarly well, the simplest model is preferred, since the sigmoid will reduce the effective fitness of the more complex one. As was mentioned earlier, our goal is to characterize the SUT by fitting the model that contains as small number of free parameters as possible, while providing good fit. IS-GP has the potential to create composite nonlinear models. However, the main goal is that IS-GP enables to evolve complex but not over-fitted models. This goal is attained by correctly choosing the constants λ and β in order to penalize some complicated solutions and to encourage simple ones, as well as by reducing the value of α in Eq. 11, as this will reduce the fitness of over-trained models.

The model complexity calculation takes into account the mathematical functions and terminals that appear in the optimized model and do not include all the model constants. All mathematical functions and the power terminals contribute unity to the overall complexity calculation, while all the other terminals contribute two. For example, the complexity of the model presented in Fig. 4 (right hand side) is 10. A discrepancy-complexity chart [47] that represents a merit function (based on the fitness of a suggested model) versus the model complexity is displayed in addition to the regular Cole–Cole and other plots. The best models are those that reside in the vicinity of the knee in this chart, i.e., have low discrepancy and low complexity.

4 Results

The developed software was tested (a) on synthetic impedance data sets that were produced to test the sensitivity of the proposed technique and to estimate convergence times; and (b) on experimental impedance data obtained from measurements that were done on a dielectric sample of $BaTiO_3$ doped with Niobium [48].

4.1 Synthetic data case studies

A logarithmically-distributed set of frequencies spread over several decades of magnitude was created with the intervals as in a typical impedance experiment. The DRT function of Eq. 7 as well as the Voigt model [46] were used along with Eq. 6 to produce resistive and reactive components of the impedance data, initially without noise and subsequently, with up to 5% randomly distributed noise. Later, two logarithmic-distributed frequency sets of the impedance were produced using MathCAD® software and Eq. 8. Differences between these data sets are in random normally distributed noise, which was added to the impedance signal. The parameters of this last model are listed in Table 1.

4.1.1 Kramers–Kronig transforms results

The Voigt model supplies transformable impedance data; therefore, it was employed to estimate the accuracy of the algorithm to compute the K–K relations. Figure 5 illustrates the Voigt equivalent circuit that was used to produce the impedance data. The data were created in the typical frequency bandwidth as it is supplied by the IS experiment with 10 and 20 equally spaced intervals per decade. At this stage, noise was not added to the data and the numerical accuracy of the computation algorithm was tested. The results of the original data and its K–K transform are presented in Fig. 6. This case study tests the accuracy of the Real-to-Imaginary, the Imaginary-to-Real and the polarization resistance computations. The errors result primarily from the numerical integration scheme as well as round-off errors, and were quantified by applying AE. The average errors of the transforms are listed in Table 2. Figure 6 shows that the K–K relations software can provide the complimentary impedance data well.

4.1.2 IS-GA case study results

The IS-GA was implemented with the parameters that are listed in Table 3. Search limits for the model parameters, that is, three model parameters of each Gaussian and one of the m-CNLS parameters (ϕ, see Eq. 9) when it is not a constant predetermined by the user, should be set. The search limits for the relaxation time positions (τ_{0i}) can be

Table 3 Values of the IS-GA constants and parameters used to fit the synthetic data.

Parameter	Value
Number of the algorithm implementations	3
Population size	100
Number of generations per implementation	50
Probability of mutation	0.05
Initial score limit	50
Weighting factor (b, Eq. 9)	0.8

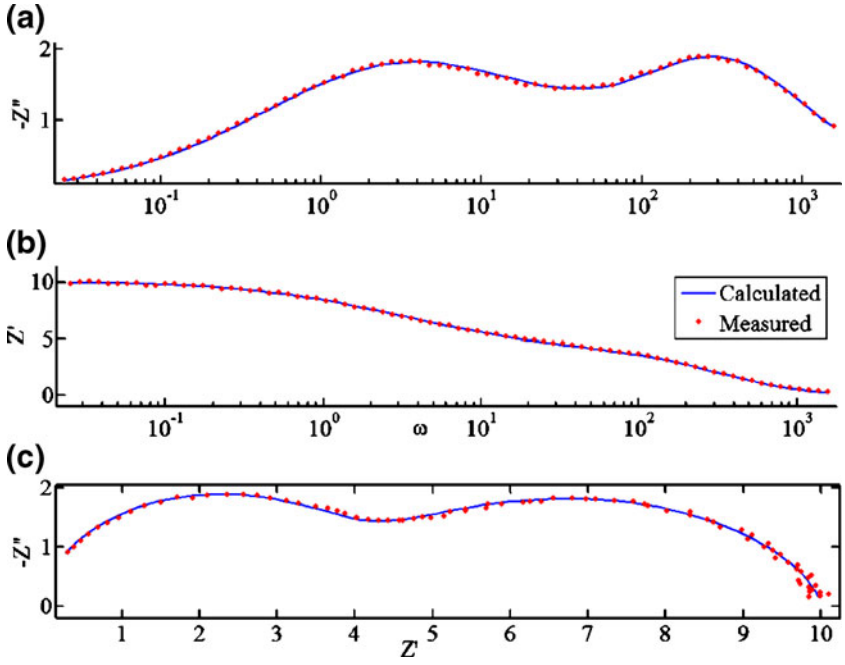

Fig. 7 Calculated by the IS-GA and measured impedance spectra of the synthetic data set with 3% noise: (**a**) the impedance imaginary part vs. logarithmic angular frequency, (**b**) the impedance real part vs. logarithmic angular frequency, (**c**) the Cole–Cole diagram

selected in one of two ways. The first alternative is to determine them directly through observation of the imaginary component of the impedance versus logarithmic scaled frequency. This case is practical only in situations when the peaks of the relaxation times are sufficiently distinct and, hence, the relaxation time boundaries of each Gaussian can be approximately determined. The second alternative determines the whole range of frequencies as the boundaries of each Gaussian.

The results of the fitting process of the data set including 3% normally distributed noise are presented in Fig. 7, where the dotted lines show the synthetic data and the continuous line represents the fitted model. Tables 4 and 5 list the fitted model parameters and the deviations between the genuine and calculated values after 50 generations. The convergence improvement during the generations is presented in Fig. 8. The m-CNLS criterion decreases by about four orders of magnitude and can decrease more. One can clearly observe in Fig. 8 that even after 50 generations the convergence criterion still descends steadily.

The case study demonstrates the ability of IS-GA to fit the synthetic data with normally distributed random noise that pass the K–K transforms adequately. The advantage of the algorithm is that the user does not require setting close enough boundary values of the parameters because the GA chooses them by itself. The algorithm requires little time to converge (seconds or minutes) and the convergence is very significant.

Table 4 Values of the IS-GA fitted parameters of the synthetic data (Eq. 8, genuine data from Table 1 with 3% random noise).

ρ_i	σ_i	$\log_{10}(\tau_{0i})$	ϕ	R_{pol}	m-CNLS
0.6608	0.7133	−0.5345	0.0933	9.8337	0.0173
0.4171	0.2660	−2.5221			

4.1.3 IS-GP case study results

The next step of the evolutionary programming implementation was to test the IS-GP code on synthetic data with noise. Values of the IS-GP parameters that need to be defined before the implementation of the algorithm are listed in Table 6; note that these values were kept constant. In GP, the population size is generally selected to be significantly lower than that selected for a GA. The reason is that the GP computation time is drastically longer than GA's because of the large number of mathematical operations.

Table 5 IS-GA case study: deviation between the genuine and calculated values of the model parameters.

Parameter	Error [%]
ρ_1	10.13
σ_1	1.90
$\log_{10}(\tau_{01})$	6.90
R_{pol}	1.66
ρ_2	4.20
σ_2	11.33
$\log_{10}(\tau_{02})$	0.88

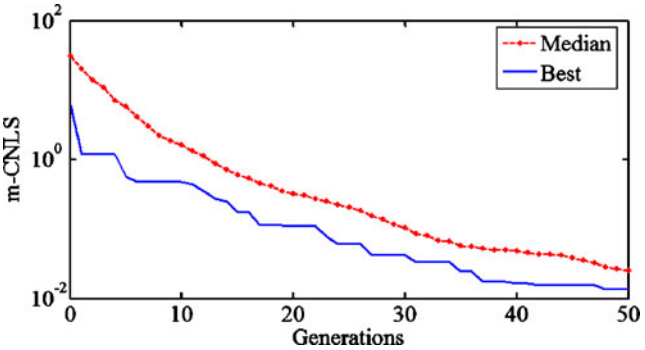

Fig. 8 Discrepancy-complexity plot for the IS-GA case study: decreasing of the convergence criterion during evolution process of the synthetic data

Table 6 Internal values of the IS-GP parameters in Section 4.1.3.

Genetic programming parameters	
Number of implementations	2
Number of generations	50
Population size	20
Crossover probability	0.3
Mutation probability	0.4
Permutation probability	0.3
Probability of a constant to mutate into an input	0.4
Fitness function parameters (Eq. 11)	
λ	3
β	3
Initial population parameters	
Maximum number of sub-trees	12
Probability to create a sub-tree	0.4

The best model generated by the IS-GP algorithm is presented in Eq. 12 and is shown in Fig. 9:

$$\Gamma(x) = -5.33 \cdot exp^{-\left(\frac{2.5+x}{0.422}\right)^2} - 3.44 \cdot exp^{-\left(\frac{0.5+x}{0.986}\right)^2} \quad (12)$$

where $x=\log_{10}(\tau)$. The figure shows the behavior of the proposed distribution of relaxation time function at the specified discrete data points. The solid line in Fig. 9 shows the extrapolated function to plus and minus "infinity". Function extrapolation shows the asymptotic behavior of the suggested DRT model: vanishing at extreme limits of frequency, positive at all relaxation times, real and continuous. Figure 10 shows the impedance that is calculated by the integration of Eq. 6 and the proposed DRT function (solid line) along with the two sets of data that have been used. The first data set that was used to determine the model's parameters and the modeling fitness, f_M, and the second data set that was used for validation and to determine the prediction fitness, f_P. Each of these sets contains 3% of randomly added noise. Eq. 12 can be expressed according to Eq. 8. In this form, the model parameters are presented in Table 7 along with the deviation between the actual parameter values (Table 1) and those computed by the IS-GP. Herein, ρ_i^* indicates the height of the Gaussian (ρ_i) multiplied by the polarization resistance, R_{pol}. It can be seen from the real part plot of Fig. 10 that the polarization resistance, where the frequency approaches zero, equals ten.

The merit function estimates the fitness, or discrepancy between the data and the fitted model for a particular selection of the parameters, on a log scale. Figure 11 demonstrates the typical behavior of the GP code. The GP model generator chooses the first population, Fig. 11(a), randomly. It leads to the creation of models with different complexities and high discrepancy values. In the next step, the GP code reduces the unnecessary complexity and produces simpler but better-fitting models that are shown in Fig. 11(b) for the 10th generation. In subsequent generations, GP reproduces the models by adopting the more suitable functions from the preceding generation and improves its population fitness as can be seen from Fig. 11(c–d) for generations 20 and 30 respectively. At later generations, the distribution of the particular model complexity is narrow as can be clearly observed in Fig. 11(e–f) for generations 40 and 50 respectively. As in the previous case, the best model is defined as the simplest, adequately-fitted function and is marked by the cross in Fig. 11(f).

4.2 Experimental case studies

Niobium-doped $BaTiO_3$ samples were produced by two different techniques and IS was employed to measure the electrical behavior of the material at several temperatures [48]. The first method results in a more uniform sample, which is hereafter referred to as "Sample-U" while the second method results in a core-shell sample, which is referred to as "Sample-CS".

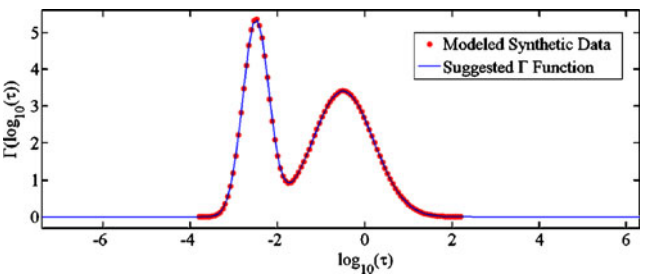

Fig. 9 The DRT function fitted by IS-GP (Eq. 12)

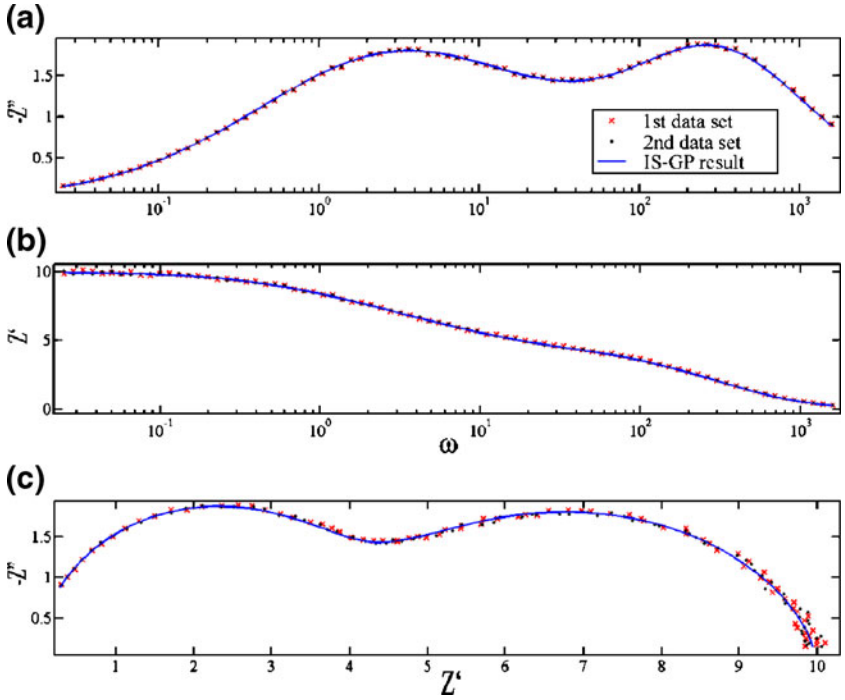

Fig. 10 Calculated and measured impedance spectra of the noisy synthetic data sets. The first data set is used to determine the model's parameters and the modeling fitness, f_M. The second data set is used for validation and to determine the prediction fitness, f_P. (**a**) The impedance imaginary part vs. logarithmic angular frequency. (**b**) The impedance real part vs. logarithmic angular frequency. (**c**) The Cole–Cole diagram

4.2.1 Kramers–Kronig transforms results

As the first stage in the analysis of the experimental IS data, the Kramers–Kronig validation test was employed. The data were measured in five different temperatures between 275°C and 375°C with intervals of 25°C. Figure 12 shows the results of the K–K transforms, where the data are presented by dotted lines and their K–K transforms by solid lines. It can be seen that the data measured at 275°C do not exhibit a local maximum in the imaginary component, which is a difficulty here. At all other temperatures, the measured sets do have local maxima, but do not reduce to zero at $\omega \rightarrow 0$. Thus, the differences between the measured data and their K–K transforms result from insufficient measured frequency bandwidth and numerical computation errors. The majority of discrepancy occurs at low frequencies and can be explained by the long measured period. As a result, the properties of the SUT can be changed during the experiment, while the averaging is done over fewer periods. For example, about 17 min are required to measure the impedance at frequency 10^{-3} Hz. Furthermore, in such long experiments, the environment can also affect the experimental measurements. For example, the influence of the contact quality between the electrodes and the sample and fluctuations of temperature during the experiment, may have influence on the results.

Table 7 Gaussian model parameters and their deviations between the genuine and calculated values of the IS-GP fitted model derived from Eq. 8.

ρ_i^*	Error [%]	σ_i	Error [%]	$\log_{10}(\tau_{0i})$	Error [%]
6.010	0.17	0.6970	0.43	−0.5	0
3.995	0.13	0.2988	0.4	−2.5	0

4.2.2 IS-GA case study results

This section presents the IS-GA fitting results of sample-CS at various temperatures between 275°C and 375°C. Figure 13 demonstrate the matching of the measured and modeled components of the data fitted by Eq. 8. The IS-GA was carried out with the parameters listed in Table 8. A model that is superposition of two Gaussian was employed as the DRT function. The selection of the relaxation time boundaries was based on the imaginary impedance component in order to reduce the search space and time.

Before the computation, an initial population is created by defining the minimum and maximum limits of the model. The boundary limits of the Gaussians' height lie between zero and four. The random number generator of

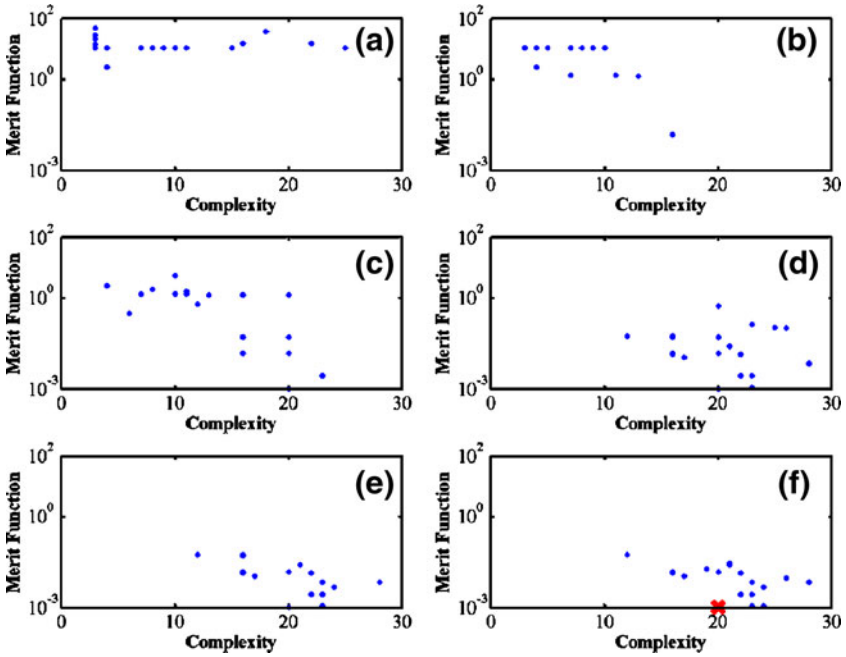

Fig. 11 The merit function vs. complexity of all of the suggested models: (**a**) 1st, (**b**) 10th, (**c**) 20th, (**d**) 30th, (**e**) 40th and (**f**) 50th generations

Matlab® creates the initial population parameters. The value of the standard deviation (σ_i) can be chosen within the same boundaries. The definition of the relaxation time boundaries is based on the imaginary impedance component (first alternative). Table 9 summarizes the results of the IS-GA implementations. It can be seen that the superposition of two Gaussian distribution functions can model the experimental data of the $BaTiO_3$ sample-CS well.

4.2.3 IS-GP case studies results

The previous section shows that the Gaussian distribution function can model the experimental $BaTiO_3$ data. However, is it possible to find a more compact model with less number of free parameters that can fit the data as good as the Gaussian function does? The Sample-U set that was measured at 325°C was chosen to be fitted by IS-GP. The data that this sample produces look like a single, yet distributed, process. The IS-GP was carried out with the parameters that are listed in Table 10.

In this case study, the influence of the initial guess model was examined by numerous implementations of the IS-GP code with different initial models. To initiate the evolutionary algorithm, a feasible DRT model must be supplied by the user. The Gaussian distribution function fulfills the feasibility conditions and fits the experimental data adequately. Therefore, it was used as the initial guess in the first implementation of the code as shown in Fig. 14 by model A. Later, a superposition of two Gaussians, model B, was employed in order to examine the ability of the genetic programming to reduce the complexity of the initial model. (Other initial guesses, including even constant distribution, where also tried, always with similar result). As illustrated in Fig. 14, in both cases the IS-GP algorithm converged to the same model containing an enlarged version of the Gaussian (centered model in Fig. 14). The best-fitted GP model is presented in Eq. 13:

$$\Gamma(x) = 542 \cdot \left(1,135 \cdot \left(exp\left(-(0.89+x)^2\right)\right)^4\right)^2 \tag{13}$$

where $x=\log\tau$. More simplification, reduction and combination of this equation are advisable and it could be rewritten in the form of Eq. 7 as demonstrated in Eq. 14:

$$\Gamma(x) = 4.377 \times 10^8 \cdot \frac{1}{\sqrt{2\pi\left(1/4\right)}} \cdot exp\left(-\frac{(0.89+x)^2}{2\cdot\left(1/4\right)^2}\right) \tag{14}$$

Figure 15(a) shows the fitted DRT model in the experimentally measured points and the continuous line in Fig. 15(b) represents the interval in which the integration occurs. The same experimental data were fitted by the IS-GA and the results of both fits are presented in Fig. 16. The IS-GP and IS-GA fitted parameters and the discrepancies between these two techniques are listed in Table 11. The m-CNLS value was calculated by Eq. 9 with the following parameters: ϕ=0.5493 and b=0.6. From Fig. 16 and

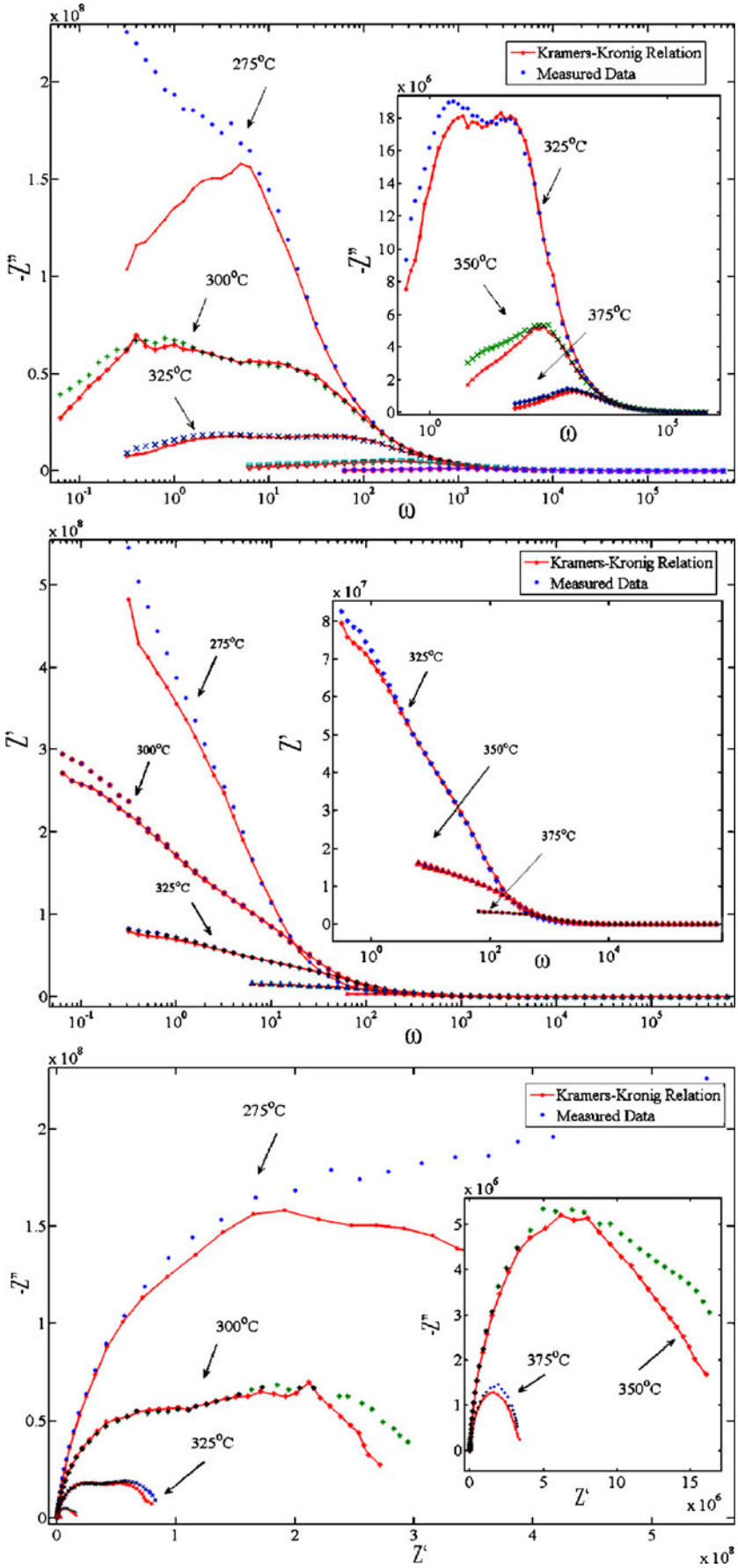

Fig. 12 K–K calculated and measured impedance spectra of $BaTiO_3$ Sample-CS at various temperatures: the imaginary part, the real part and the Cole–Cole diagram

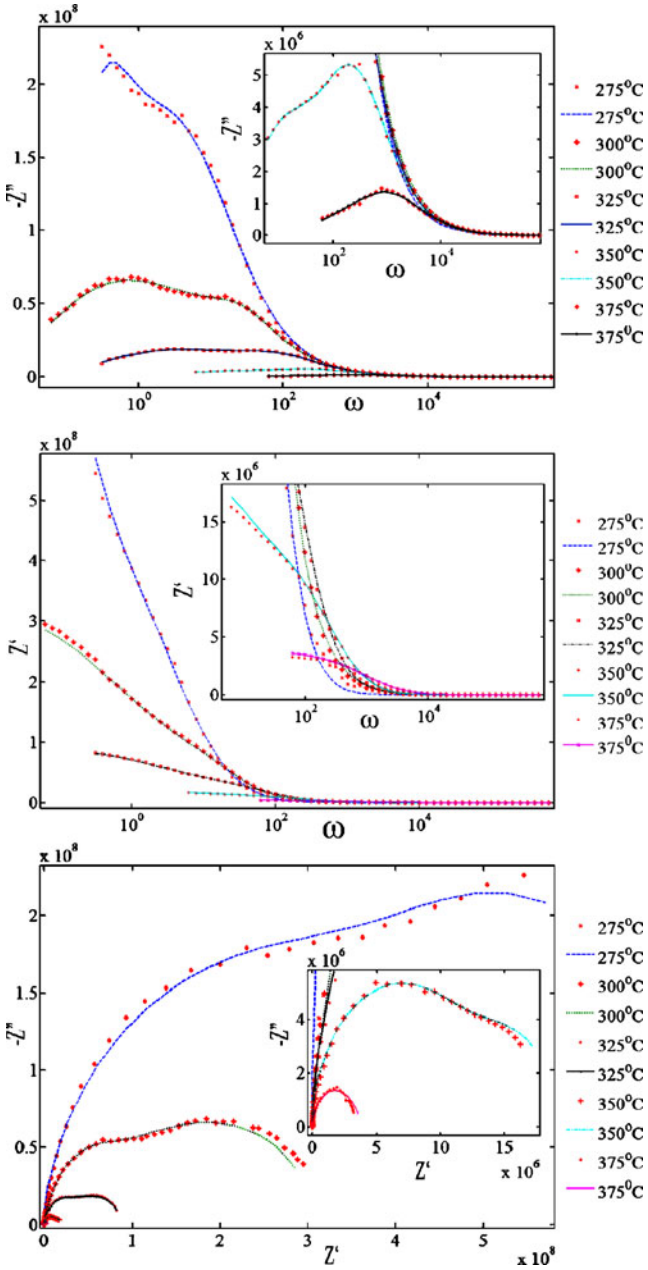

Fig. 13 Calculated and measured impedance spectrum of $BaTiO_3$ Sample-CS at various temperatures: the reactive impedance component, the resistive impedance component and the Cole–Cole diagram

Table 8 The IS-GA constants and parameters used to fit the experimental $BaTiO_3$ sample-CS data.

Parameter	Value
Number of the algorithm implementations	1–3
Population size	100
Number of generations per implementation	50–300
Probability of mutation	0.05
Initial score limit	10–100
Weighting factor (b, Eq. 9)	0.6–0.9

Table 9 The fitted model parameters of the $BaTiO_3$ Sample-CS at 275–375°C.

T	ρ_i	σ_i	$\log_{10}(\tau_{0i})$	R_{pol}	ϕ	m-CNLS
275	0.7876	0.5184	−0.5898	5.5569×10^8	1.0563	0.0847
	0.8585	0.0375	0.5553			
300	0.1600	0.0918	−1.4570	2.7903×10^8	1.4207	0.0412
	1.1101	1.0940	0.2497			
325	0.2607	0.2506	−1.9776	8.0073×10^7	0.8105	0.0354
	0.9581	0.9550	−0.4140			
350	0.6968	0.3433	−2.4057	1.6716×10^7	0.2329	0.0259
	0.9187	0.5985	−0.6591			
375	0.9000	0.3750	−3.0144	3.4927×10^6	0.8784	0.1168
	0.9999	0.8794	−0.9282			

Table 11 it can be seen that in both fitting methods the parameters of the models are similar.

5 Conclusions

This work has introduced a new concept to analyze IS results by employing evolutionary programming techniques. The noteworthy potential of the IS-GA and IS-GP has been demonstrated. The implementation of the IS-GP code would appear to be particularly advantageous when the analyses of new systems are called for, and in these cases the significantly longer computation times are justified. Subsequently, after the GP has identified appropriate functional representations of prediction model, the IS-GA can be harnessed to perform robust parameter identification for similar systems. Additionally, this work has shown that the GP can solve the IS inverse problem; by providing it a library of alternative different kernel functions to be used to seed appropriate model, and defining conditions and constrains that need to be satisfied, the GP can be used as a "universal" solver for other inverse problems.

Table 10 The IS-GP parameters that remain fixed during calculation.

Genetic programming parameters	
Number of implementations	2
Number of generations	40–50
Population size	15–20
Crossover probability	0.3
Mutation probability	0.4
Permutation probability	0.3
Probability of a constant to mutate into an input	0.4
Fitness function parameters (Eq. 11)	
λ	3
β	3
Initial population parameters	
Maximum number of sub-trees	12
Probability to create a sub-tree	0.4

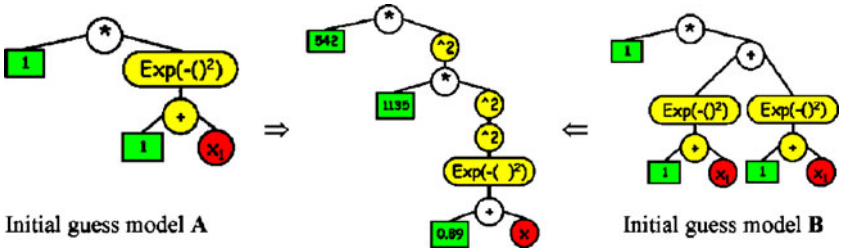

Fig. 14 Two different models (*A* and *B*) used as the initial guess in the IS-GP in two different implementations and the best-fitted model (in center)

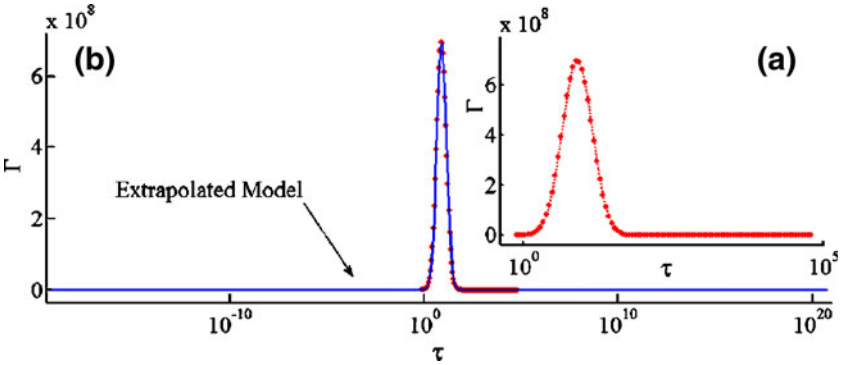

Fig. 15 DRT model of $BaTiO_3$ Sample-U at 325 °C temperature: (**a**) DRT function in the measured frequency interval and (**b**) extrapolated DRT function as it is integrated in the IS-GP

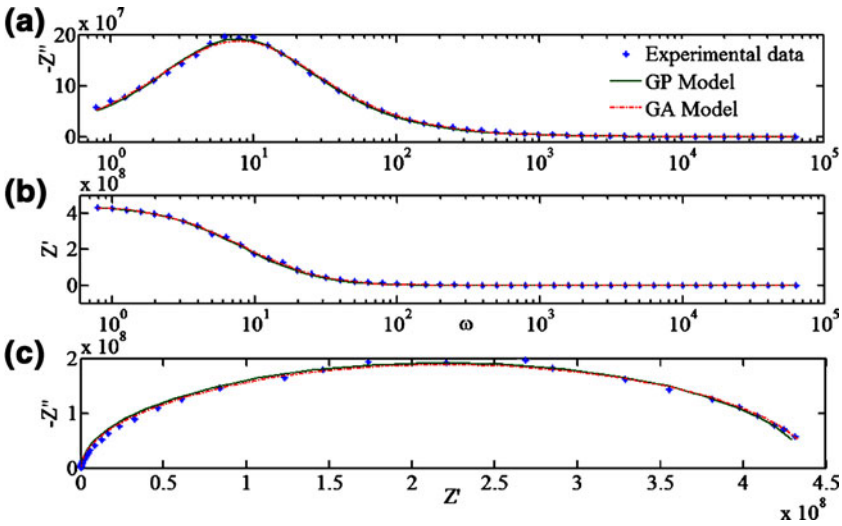

Fig. 16 GA and GP calculated and measured impedance spectrum of $BaTiO_3$ Sample-U at 325°C temperature: (**a**) the reactive and (**b**) the resistive impedance components vs. angular frequency in logarithmical scale, (**c**) the Cole–Cole diagram

Table 11 The fitted model parameters of the $BaTiO_3$ sample-U at 325°C.

Technique	ρ_i	σ_i	$\log_{10}(\tau_{0i})$	R_{pol}	m-CNLS
IS-GA	1.0688	0.2829	−0.8951	4.3770×10^8	0.0779
IS-GP	1.0000	0.2500	−0.8900	4.1406×10^8	0.1069
Deviation [%]	6.44	11.63	0.57	5.40	

Acknowledgements Partial funding of the Technion's Fund for Promotion of Research and the I. Goldberg Fund for Electronic Research are gratefully acknowledged. S.B. would like to acknowledge the support of The Center for Absorption in Science, Israeli Ministry of Immigrant Adsorption. We would also like to thank an anonymous reviewer for very thorough reading of the manuscript and useful suggestions.

Appendix: Calculations of average error

The finite frequency bandwidth of the experiment causes a major difficulty to the implementation of K–K transforms and produces an inherent inaccuracy in the calculation algorithm. Additional inaccuracy of K–K transforms is originated in numerical integration scheme. In order to determine the validity of the measured impedance data, Average Error (AE) was defined as follows:

$$\mathrm{AE} = 100 \cdot \frac{\sum_{i=1}^{N} \left| Z^i_{\mathrm{meas}}(\omega) - Z^i_{\mathrm{KKT}}(\omega) \right|}{N \cdot Z_{\mathrm{meas,max}}} \qquad (15)$$

where Z_{meas} and Z_{KKT} are the values observed experimentally and calculated by K–K transform. $Z_{\mathrm{meas,max}}$ is the maximum value of the experimental relevant data set (real or imaginary) and N is the total number of measured points. Normalization of Eq. 15 by $Z_{\mathrm{meas,max}}$ enables the comparison of the different data sets that can differ by orders of magnitude.

References

1. J.R. Macdonald, *Impedance Spectroscopy: emphasizing solid materials and systems* (Wiley, New York, 1987)
2. B.A. Boukamp, Electrochemical impedance Spectroscopy in Solid State Ionics: recent advances Solid State Ion. **169**, 56 (2004) doi:10.1016/j.ssi.2003.07.002
3. W.A. Yager, The Distribution of Relaxation Times in Typical Dielectrics Physics **7**, 434 (1936) doi:10.1063/1.1745355
4. X. Li, Impedance Spectroscopy for Manufacturing Control of Material Physical Properties, Thesis, University of Washington (2003)
5. R. Lantham, Algorithm Development for Electrochemical Impedance Spectroscopy Diagnostics in PEM Fuel Cells, Thesis, University of Victoria (2004)
6. A.J. Jonscher, The Universal Dielectric response and its Physical Significance IEEE Trans. Electr. Insul. **27**, 407 (1992) doi:10.1109/14.142701
7. C.J. Dias, Determination of a distribution of relaxation frequencies based on experimental relaxation data Phys. Rev. B **53**, 212 (1996) doi:10.1103/PhysRevB.53.14212
8. F. Mansfeld, H. Xiao, Y. Wang, Evaluation of localized corrosion phenomena with electrochemical impedance spectroscopy and electrochemical noise analysis Mater. Corros. **46**, 3 (2004)
9. K.E. Jeffers, Electrochemical impedance spectroscopy for the characterization of corrosion and cathodic protection of buried pipelines, Thesis, University of Florida (1999)
10. G. Rocchini, The corrosion-trend monitoring with the impedance technique Mater. Corros. **49**, 18 (1998) doi:10.1002/(SICI)1521-4176(199801)49:1<18::AID-MACO18>3.0.CO;2-R
11. W.H. Press, S.A. Teukolsky, W.T. Vetterling, B.P. Flannery, *Numerical Recipes in C: The Art of Scientific Computing* (Cambridge University Press, Cambridge, 2002)), p. 788
12. S. Baltianski, Y. Tsur, Analyzing impedance spectroscopy results Rare Met. Mater. Eng. **35**(Suppl. 3), 452 (2006)
13. J. Macutkevic, J. Banys, A. Matulis, Determination of the Distribution of the Relaxation Times from Dielectric Spectra Nonlinear Anal. Model. Contr. **9**, 75 (2004)
14. E. Tuncer, S.M. Gubanski, On dielectric data analysis IEEE Trans Dielectr Electr Insul **8**, 310 (2001)
15. H. Schichlein, A.C. Müller, M. Voigts, A. Krügel, E. Ivers-Tiffée, Deconvolution of electrochemical impedance spectra for the identification of electrode reaction mechanisms in solid oxide fuel cells J. Appl. Electrochem. **32**, 875 (2002) doi:10.1023/A:1020599525160
16. M. Urquidi-Macdonald, D.D. Macdonald, Application of Kramers–Kronig Transforms in the Analysis of Electrochemical Systems J. Electrochem. Soc. **132**, 2316 (1985) doi:10.1149/1.2113570
17. H. Cao, J. Yu, L. Kang, An evolutionary approach for modeling the equivalent circuit for electrical impedance spectroscopy, in *Proceedings of the 2003 Congress on Evolutionary Computation*, Canbera, Australia, 1819, IEEE (2003)
18. Gamry Instruments Inc., *Equivalent Circuit Modeling Using the Gamry EIS300 Electrochemical Impedance Spectroscopy Software* (Gamry Instruments Inc.,, Warminster, PA, 2003)
19. T.J. Van der Noot, I. Abrahams, The use of genetic algorithms in the non-linear regression of immittance data J. Electroanal. Chem. **448**, 17–23 (1998) doi:10.1016/S0022-0728(97)00593-7
20. M. Yang, X. Zhang, X. Li, X. Wu, A hybrid genetic algorithm for the fitting of models to electrochemical impedance data J. Electroanal. Chem. **519**, 1–8 (2002) doi:10.1016/S0022-0728(01)00707-0
21. H. Cao, J. Yu, L. Kang, *An Evolutionary Approach for Modeling the Equivalent Circuit for Electrical Impedance Spectroscopy, Congress on Evolutionary Computation* (IEEE, Canberra, 2003)
22. M. Orazem, P. Agarwal, L.H. Garcia-Rubio, Critical issues associated with interpretation of impedance data J. Electrochem. Chem. **378**, 51 (1994) doi:10.1016/0022-0728(94)87056-X
23. A.R. West, D.C. Sinclair, N. Hirose, Characterization of Electrical Materials, Especially Ferroelectrics, by Impedance Spectroscopy J. Electroceram. **1**, 65 (1997) doi:10.1023/A:1009950415758
24. J. Fleig, Impedance Spectroscopy on Solids: The Limits of Serial Equivalent Circuit Models J. Electroceram. **13**, 637 (2004) doi:10.1007/s10832-004-5170-3
25. P. Nordin, W. Banzhaf, R.E. Keller, F.D. Francone, *Genetic Programming: An Introduction: on the Automatic Evolution of Computer Programs and Its Applications* (Kaufmann, Los Altos, CA, 1998)
26. J.R. Koza, *Genetic programming* (MIT, Cambridge, 1992)
27. J.M. Link et al., Application of genetic programming to High Energy Physics event selection, **551**, 504–527 (2005), Los Alamos National Laboratory, High Energy Physics Experiment
28. D.E. Makarov, H. Metiu, Using Genetic Programming to solve the Schrödinger Equation J. Phys. Chem. A **104**, 8540 (2000) doi:10.1021/jp000695q
29. K. Sastry, D.D. Johnson, D.E. Goldberg, P. Bellon, Genetic Programming for Multiscale Modeling Int. J. Multiscale Comput. Eng. **2**, 239 (2004) doi:10.1615/IntJMultCompEng.v2.i2.50
30. S.J. Barrett, W.B. Langdon, Advances in the application of machine learning techniques in drug discovery, design and development, in *10th Online World Conference on Soft Computing in Industrial Applications*, Springer (2005)

31. W.B. Langdon, S.J. Barrett, Genetic programming in data mining for drug discovery Evol. Comput. Data Min. **163**, 211 (2004) doi:10.1007/3-540-32358-9_10
32. B. Grosman, Nonlinear system modeling using genetic programming, Thesis, Technion-ITT (2001)
33. B. Grosman, D.R. Lewin, Adaptive genetic programming for steady-state process modeling, Comput. Chem. Eng. **28**, 2779 (2004) doi:10.1016/j.compchemeng.2004.09.001
34. Y. Melman, S. Baltianski, Y. Tsur, A device for measuring electrical properties of dielectric materials Instrum. Sci. Technol. **33**, 279 (2005) doi:10.1081/CI-200056096
35. R. De, L. Kronig, On the theory of dispersion of X-rays J. Opt. Soc. Am. Rev. Sci. Instrum. **12**, 547 (1926)
36. H.A. Kramers, La diffusion de la lumi'ere par les atomes Atti Congr. Int. Fis. Como **2**, 545 (1927)
37. A.D. Poularicas, *The Transforms and Applications Handbook* (IEEE, Canberra, 2000)
38. F.W. King, Efficient numerical approach to the evaluation of Kramers–Kronig transforms J. Opt. Soc. Am. B **19**, 2427 (2002) doi:10.1364/JOSAB.19.002427
39. H.W. Bode, *Network Analysis and Feedback Amplifier Design*, *Network Analysis and Feedback Amplifier Design* (Van Nostrand Co., New York, 1953), p. 303
40. M. Urquidi-Macdonald, S. Real, D.D. Macdonald, Applications of Kramers–Kronig transforms in the analysis of electrochemical impedance data-II. Transformations in the complex plane J. Electrochem. Soc. **133**, 2018 (1986) doi:10.1149/1.2108332
41. A. Sadkowski, Unusual electrochemical immittance spectra with negative resistance and their validation by Kramers–Kronig transformation Solid State Ion. **176**, 1987 (2005) doi:10.1016/j.ssi.2004.08.041
42. A.L. Smirnova, K.R. Ellwood, G.M. Crosbie, Application of Fourier-based transforms to impedance spectra of small-diameter tubular solid oxide fuel cells J. Electrochem. Soc. **148**(6), A610–A615 (2001) doi:10.1149/1.1372212
43. J. Zhang, P.J.M. Monteiro, Validation of resistivity spectra from reinforced concrete corrosion by Kramers–Kronig transformations Cement Concr. Res. **31**, 603 (2001) doi:10.1016/S0008-8846(01)00451-3
44. F. Alvarez, A. Alegria, J. Colmenero, Relationship between the time-domain Kohlrausch–Williams–Watts and frequency-domain Havriliak–Negami relaxation functions Phys. Rev. B **44**, 7306 (1991) doi:10.1103/PhysRevB.44.7306
45. D.D. Macdonald, Reflections on the history of electrochemical impedance spectroscopy Electrochim. Acta **51**, 1376 (2006) doi:10.1016/j.electacta.2005.02.107
46. E. Barsoukov, J.R. Macdonald, *Impedance Spectroscopy: Theory, Experiment, and Applications* (Wiley, New York, 2005)
47. S. Baltianski, Y. Tsur, Analysis of impedance spectroscopy data—finding the best system function J. Electroceram. **10**, 89 (2003) doi:10.1023/A:1025639604939
48. H. Yaseen, S. Baltianski, Y. Tsur, Effect of incorporating method of niobium on the properties of doped barium titanate ceramics J. Am. Ceram. Soc. **89**, 1584 (2006) doi:10.1111/j.1551-2916.2006.00966.x